Unveiling genetic architecture of white matter microstructure through unsupervised deep representation learning of fractional anisotropy images

Xingzhong Zhao[1], Ziqian Xie[1], Wei He[1], Myriam Fornage[2,3], Degui Zhi[1, *]

1. McWilliams School of Biomedical Informatics, University of Texas Health Science Center, Houston, TX, 77030, USA.

2. School of Public Health, University of Texas Health Science Center, Houston, TX, 77030, USA

3. McGovern Medical School, University of Texas Health Science Center, Houston, TX, 77030, USA

Abstract

Fractional anisotropy (FA) derived from diffusion MRI is a widely used marker of white matter (WM) integrity. However, conventional FA based genetic studies focus on phenotypes representing tract- or atlas-defined averages, which may oversimplify spatial patterns of WM integrity and thus limiting the genetic discovery. Here, we proposed a deep learning-based framework, termed unsupervised deep representation of white matter (UDR-WM), to extract brain-wide FA features-referred to as UDIP-FA, that capture distributed microstructural variation without prior anatomical assumptions. UDIP-FAs exhibit enhanced sensitivity to aging and substantially higher SNP-based heritability compared to traditional FA phenotypes ($P < 2.20e-16$, Mann-Whitney U test, mean $h^2 = 50.81\%$). Through multivariate GWAS, we identified 939 significant lead SNPs in 586 loci, mapped to 3480 genes, dubbed UDIP-FA related genes (UFAGs). UFAGs are overexpressed in glial cells, particularly in astrocytes and oligodendrocytes (Bonferroni-corrected $P < 2e-6$, Wald Test), and show strong overlap with risk gene sets for schizophrenia and Parkinson disease (Bonferroni-corrected $P < 7.06e-3$, Fisher exact test). UDIP-FAs are genetically correlated with multiple brain disorders and cognitive traits, including fluid intelligence and reaction time, and are associated with polygenic risk for bone mineral density. Network analyses reveal that UFAGs form disease-enriched modules across protein-protein interaction and co-expression networks, implicating core pathways in myelination and axonal structure. Notably, several UFAGs, including *ACHE* and *ALDH2*, are targets of existing

neuropsychiatric drugs. Together, our findings establish UDIP-FA as a biologically and clinically informative brain phenotype, enabling high-resolution dissection of white matter genetic architecture and its genetic links to complex brain traits.

Introduction

White matter microstructure is a critical structural component of the brain that facilitate efficient communication between distributed gray matter regions, thereby supporting essential cognitive functions such as memory, attention, and executive control[1]. Fractional anisotropy (FA) is a widely used neuroimaging quantitative measure of white matter microstructure, derived from the diffusion tensor images (DTI) [2]. FA is an important biomarker in studying brain function and brain-related disorders, as it can sensitively track the white matter changes in Alzheimer's disease (AD), distinct cognitive functions[3,4], and several neurological and psychiatric disorders[5-8]. Understanding the genetic architecture of fractional anisotropy (FA) will shed light on the biological mechanisms of individual variability in cognitive and behavioral traits, as well as susceptibility to brain disorders.

Over the past decade, advances in imaging genetics have enabled large-scale genomic studies to elucidate the genetic architecture of FA. ENIGMA DTI Working Group and the Human Connectome Project demonstrated that FA derived phenotypes across major white matter tracts exhibits moderate to high SNP-based heritability (h^2: 0.53–0.90)[9]. Subsequent genome-wide association studies (GWAS) using UK Biobank imaging data identified genome-wide significant loci—such as VCAN (*rs67827860*)—linked to FA, suggesting shared genetic influences on both FA and white matter hyperintensities[10]. A larger meta-GWAS combining the UK Biobank and CHARGE cohorts uncovered over 30 novel loci associated with FA, implicating genes involved in myelination and axonal integrity[11]. More recently, Zhao et al. analyzed diffusion MRI data from 43,802 individuals and identified 109 genomic regions related to white matter microstructure—including FA, revealing a highly polygenic architecture with regulatory enrichment in oligodendrocytes and significant genetic correlations with numerous neuropsychiatric traits[12]. Additionally, a neonatal FA GWAS highlighted early developmental genetic effects, including an intronic SNP in *PSMF1* [9].

Although these studies have revealed a part of the genetic component of FA traditional FA GWAS face several methodological limitations that constrain their ability to fully capture the genetic architecture of white matter microstructure. First, most studies rely on region- or tract-level mean FA intensity values based on predefined atlas, which substantially reduce the spatial complexity of the brain and limit the phenotypic variance explained. Second, conventional univariate GWAS typically assume linear, additive, and independent SNP effects, overlooking potential nonlinear interactions and cross-region dependencies. These limitations highlight the need for more integrative, high-dimensional approaches to advance our understanding of the genetic architecture of FA.

In this study, we developed and trained an unsupervised deep learning representation model that leverages whole-brain 3D FA images as input to derive a set of global neuroimaging phenotypes, termed UDIP-FAs. Our model is based on the UDIP framework that was successfully applied to derive heritable phenotypes from T1- and T2-FLAIR-weighted images. We then conducted a multi-stage, multivariate GWAS on UDIP-FAs to uncover its genetic underpinnings. The UDIP-FA enabled us to elucidate the functional and biological mechanisms associated with FA and to investigate the associations between UDIP-FA and brain disorders at both the phenotypic and molecular levels. Our findings suggest that UDIP-FA serves as a robust global imaging phenotype, offering enhanced sensitivity for capturing the genetic architecture of white matter and its links to neuropsychiatric and neurological disorders.

Result

An unsupervised representation framework to explore the genetic architecture of WM tracts using UDIP-FA

We developed an framework that extends unsupervised deep representation learning to white matter (WM) tracts (UDR-WM, Figure 1a). First, we trained an unsupervised 3D convolutional autoencoder on 4,914 FA images derived from UK Biobank (UKB) diffusion tensor imaging (DTI) data (75% training, 25% validation; Methods and Figure 1a). Using the pre-trained model, we extracted 128-dimensional deep representations—referred to as UDIP-FAs—from an independent UKB dataset (N = 25,875). We found that these UDIP-FA dimensions were largely independent, with an average absolute pairwise Pearson correlation of 0.082 ± 0.065. This suggests that each UDIP-FA dimension captures a distinct aspect of white matter (WM) tract structure or variation. We then developed a suite of methods to interpret and apply these representations (Figure 1b) to investigate their underlying genetic architecture (Figure 1c). Finally, we systematically examined the associations between UDIP-FAs and a wide spectrum of diseases across molecular layers, including variants, genes, proteins, drugs, and phenotypes (Figure 1d). In summary, our framework demonstrates that UDIP-FAs are reliable markers for capturing the genetic architecture of WM tracts and for uncovering diverse disease associations.

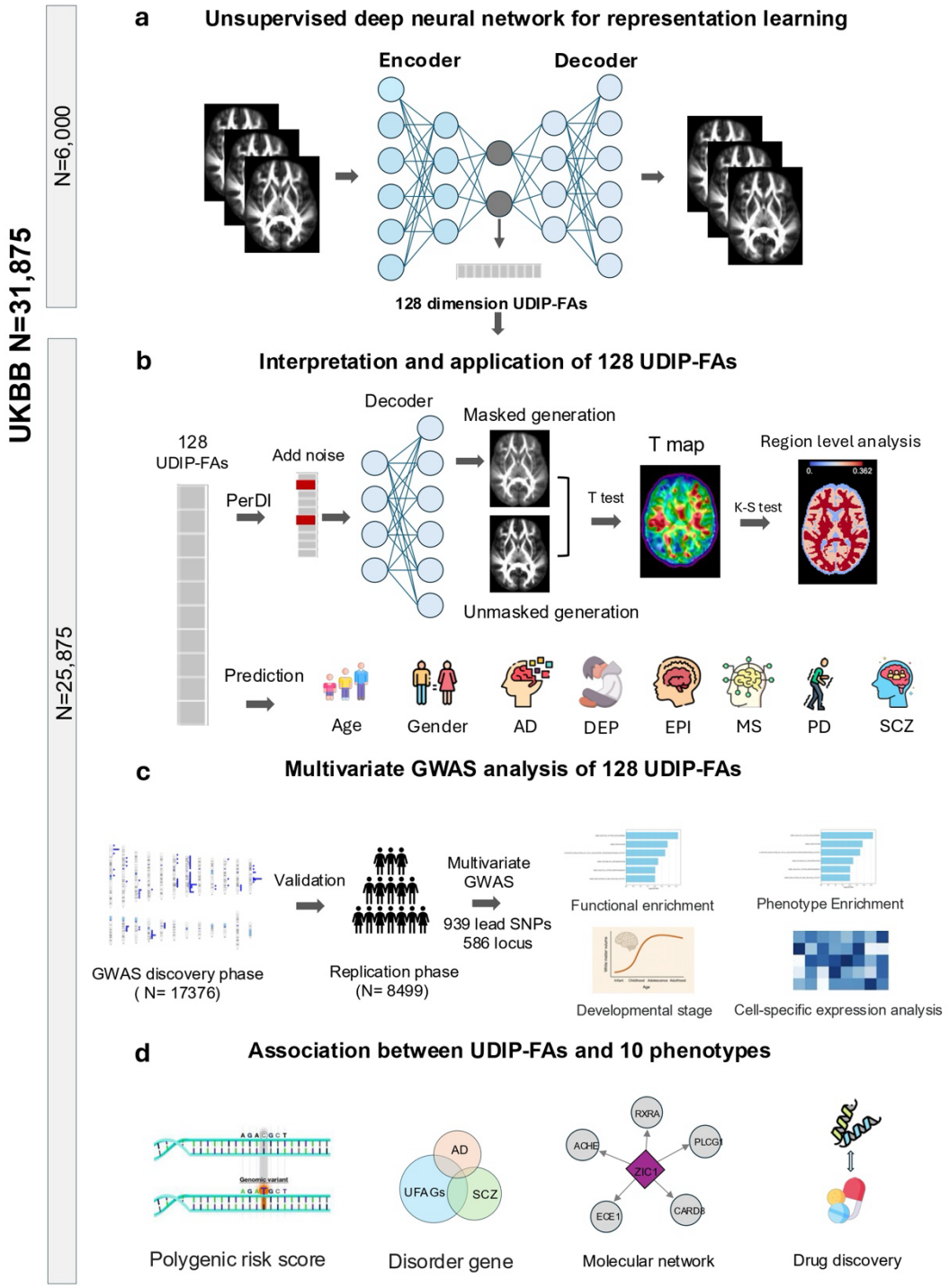

Figure: 1 Overview of the framework for UDIP-FAs. (a) Model architecture for extracting UDIP-FA. **(b)** evaluating biological meaningfulness of UDIP-FAs through interpretation and

prediction of brain-related phenotypes. **(c)** GWAS discovery pipeline of UDIP-FA. **(d)** Association between UDIP-FAs and brain disorders.

UDIP-FA characterizes the population variability of WM fiber tracts.

To explore the biological meaningfulness of UDIP-FA, first, we extracted the average FA values of 48 white matter tracts defined by a traditional approach from the UK Biobank (UKB) dataset. We then evaluated the relationship between the average FA values of each WM fiber bundle and the 128 UDIP-FA components using a multiple linear regression model (Methods). Our results showed that for all traditional WM tracts, the UDIP-FAs significantly explained population variance in FA values (Bonferroni-corrected $P < 2.2e\text{-}16$, F-test). The coefficient of determination (R^2) values ranged from 0.298 to 0.768, with a mean R^2 of 0.470 (Table S1). Then, we further evaluated the capacity of UDIP-FA to capture population-level variation in white matter microstructure, we visualized the UDIP-FA distribution using Uniform Manifold Approximation and Projection (UMAP)[13] for unsupervised dimensionality reduction. The 128-dimensional UDIP-FAs were embedded into two dimensions, and each sample was annotated with its average whole-brain FA value. As shown in Figure 2a, UDIP-FA clearly captured differences in FA values across the population, with FA values decreasing progressively from left to right.

In addition, we also explored the tissue specificity of UDIP-FA in whole brain. We employed the method of Perturbation-based decoder interpretation (PerDI, Methods)[14] to quantify the variability with which perturbed UDIP-FA can be translated into brain MRI images. With PerDI we obtained perturbed images corresponding to each UDIP-FA and then obtained UDIP-FA region-specific idiosyncratic t-statistic maps based on paired t-tests. In order to calculate the enrichment of UDIP-FAs in different tissues of the whole brain (gray matter, white matter, cerebrospinal fluid), we used the Kolmogorov-Smirnov (K-S) statistics to access the enrichment of the top 10% significant voxels in the three tissues, and we found that all of the UDIP-FAs had higher enrichment results in white matter and were significantly higher than gray matter ($P<2.2e\text{-}16$, Mann–Whitney U test) and cerebrospinal fluid ($P<2.2e\text{-}16$, Mann–Whitney U test, Figure 2b, Methods).

To elucidate the association between UDIPs and white matter tracts, we assessed the enrichment of each UDIP's t-map, derived from PerDI, within 81 white matter fiber bundles as defined by the

ICBM DTI-81 Atlas[15] (Methods). Our analysis revealed that UDIPs exhibited significant and distinct enrichment profiles across various white matter tracts (Table S2). For example, UDIP-FA dimension 1 was notably enriched in the right uncinate fasciculus (UNC-R, mean t = 20.08, Bonferroni-corrected P = 0.005, permutation test) and the genu of the corpus callosum (GCC, mean t = 23.34, Bonferroni-corrected P = 0.005, permutation test). Conversely, UDIP-FA dimension 2 showed significant enrichment in the right medial lemniscus (ML-R, mean t = 28.67, Bonferroni-corrected P = 0.001, Permutation test) and the middle cerebellar peduncle (MCP, mean t = 27.52, Bonferroni-corrected P = 0.01, permutation test).

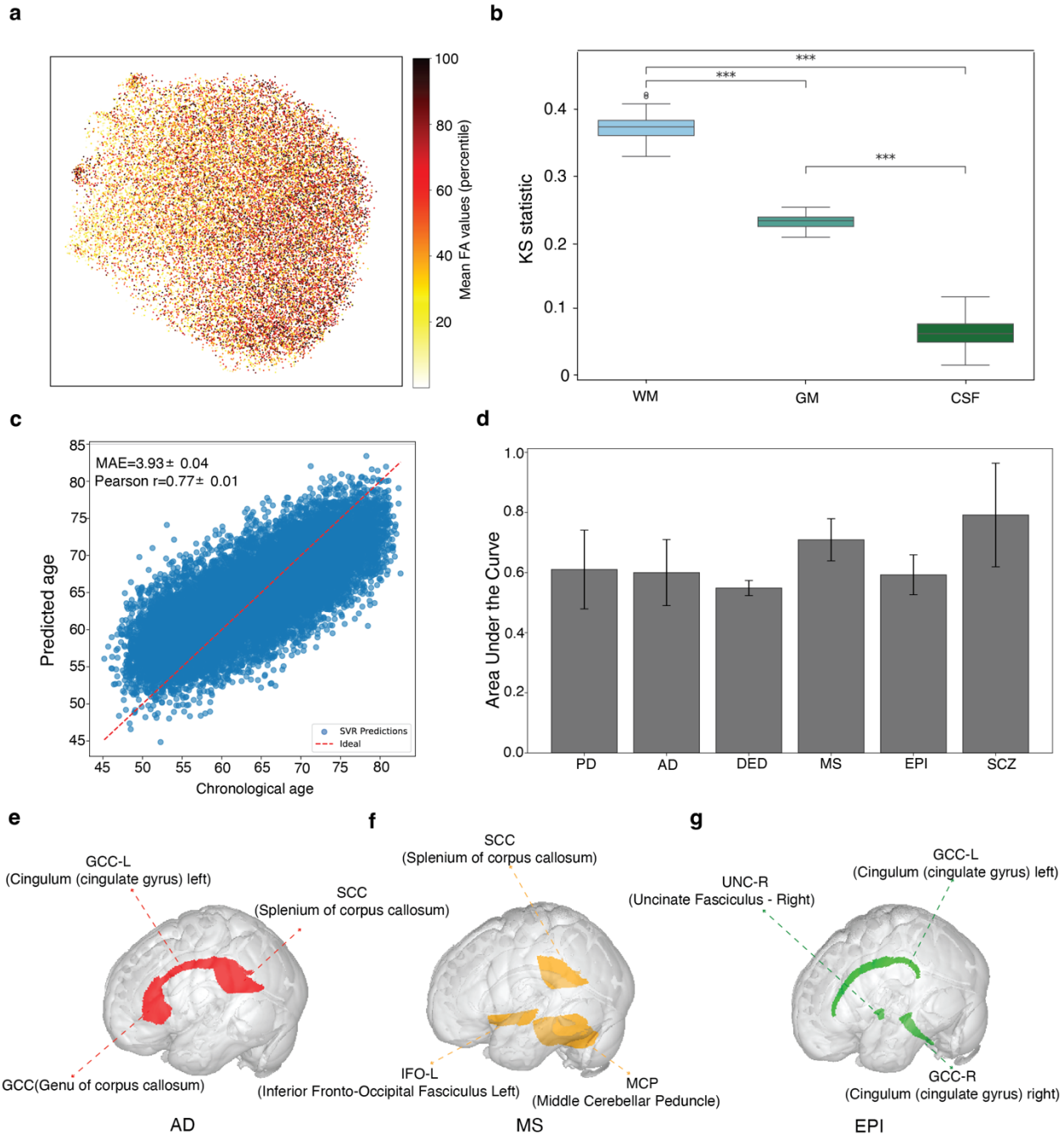

Figure 2: Characterization and clinical relevance of UDIP-FA features. (a) 2D UMAP projection of UDIP-FA representations across all subjects, colored by average mean FA values. (b) Kolmogorov–Smirnov (KS) statistics quantifying the distinctiveness of UDIP-FA features across three major tissue types: white matter (WM), gray matter (GM), and cerebrospinal fluid (CSF). WM regions exhibited significantly higher KS scores, indicating stronger discriminative

patterns (***P < 0.001). **(c)** Brain age prediction using UDIP-FA features. Scatter plot shows predicted versus chronological age, with a mean absolute error (MAE) of 3.93 years and Pearson correlation of r = 0.77. (d) Classification performance (AUC) of UDIP-FA in distinguishing individuals with various brain disorders, including Parkinson's disease (PD), Alzheimer's disease (AD), Depression (DEP), multiple sclerosis (MS), epilepsy (EPI), and schizophrenia (SCZ). **(e–g)** Brain regions identified as most predictive for AD (e), MS (f), and EPI (g) using feature importance of top 3 features from the GBDT classification model.

UDIP-FA demonstrates predictive power for age, sex, and neurological disorders.

To investigate the informativeness of UDIP-FA, we first evaluated its performance in sex and age prediction using 25,875 samples. For sex classification, we employed a Support Vector Machine (SVM) with five-fold cross-validation, achieving high accuracy (Area Under the ROC Curve (AUC) = 0.987 ± 0.001). For age prediction, a Support Vector Regression (SVR) model was used with the same training strategy. UDIP-FA demonstrated strong sensitivity to age (MAE = 3.93 ± 0.04, Pearson's r = 0.77 ± 0.01; Figure 2c), outperforming a previously published study that used the traditional FA value from different WM regions[16].

In addition, we evaluated the ability of UDIP-FA to predict the status of six brain disorders: Alzheimer's Disease (AD), Depression (DEP), Epilepsy (EPI), Multiple Sclerosis (MS), Parkinson's Disease (PD), and Schizophrenia (SCZ). Patients with these conditions were identified from the UK Biobank (UKB) dataset using ICD-10 diagnostic codes(Field 41270). A Gradient Boosting Decision Tree (GBDT) model was then applied to classify the disorder status based on UDIP-FA features (Methods). The results demonstrated that UDIP-FAs could be predictive across distinct brain disorders, achieving an average classification performance with an AUC of 0.642 ± 0.082 (Figure 2d). Furthermore, we assessed the feature importance of the classification model for each disorder to identify disorder-specific signatures. We found that key UDIP-FA features identified by the classification model can reveal potential white matter tract involvement across distinct brain disorders (Figure 2e, f, g). In AD, the critical UDIP-FA feature (*dimension_6*) was significantly enriched in the left cingulum (cingulate gyrus) (CGC-L), the genu of the corpus callosum (GCC), and the splenium of the corpus callosum (SCC), with a Bonferroni-corrected *P*

= 0.009 based on permutation test results from PerDI. These white matter tracts have previously been implicated in AD-related pathology[17,18]. In MS, the key UDIP-FA feature (*dimension_9*) showed significant enrichment in the left inferior fronto-occipital fasciculus (IFO-L, Bonferroni-corrected P = 0.009, Permutation test) and the middle cerebellar peduncle (MCP, Bonferroni-corrected P = 0.008, Permutation test), both of which have been associated with demyelination and disrupted connectivity in MS[19]. For EPI, the most prominent UDIP-FA feature (*dimension_116*) was significantly enriched in the right uncinate fasciculus (UNC-R, Bonferroni-corrected P = 0.010, Permutation test). This tract has been linked to seizure propagation and altered connectivity in epilepsy[20].

UDIP-FA exhibited greater heritability and identified more genetic loci than conventional white matter phenotypes

We used the GCTA (Genome-wide Complex Trait Analysis) software to estimate SNP-based heritability (h^2) for each UDIP-FA in our cohort of 25,875 individuals, quantifying the proportion of variance in each UDIP explained by common autosomal genetic variants (Methods). A total of 115 UDIP-FAs (89.8%) were significantly heritable (FDR-corrected $P < 0.05$), with heritability estimates ranging from 6.9% to 85.2% (mean h^2 = 52.0%; Fig. 3A and Table SX), 39 (30.5%) UDIP-FAs showed high heritability ($h^2 > 0.6$). The heritability of our UDIP-FAs was significantly higher than that of a previous study (mean h^2 = 34.9%, P < 2.2e-16, Mann–Whitney U test, Figure 3b). This is remarkable as our UDIP-FAs are largely uncorrelated.

To leverage the full sample for accurately identifying variants associated with white matter (WM) tracts, we employed a multi-stage GWAS analysis to ensure robust and replicable results (Methods, Fig. S1). First, for the single variants, we found 128 UDIP-FA measures that showed consistent GWAS results across discovery and republication cohorts, with a high paired genetic correlation (GC = 0.969 ± 0.152; Table S3) that evaluated by LD score regression (LDSC)[21]. Additionally, our results demonstrated significant genetic correlation with a previous GWAS of FA measures (GC = 0.294 ± 0.089, All Bonferroni-corrected P < 0.05, Table S4, Wald test)[12], which suggesting that the UDIP-FAs reliably capture the genetic architecture of FA. Our results were able to

replicate prior discoveries, with an overlap of 5 lead SNPs (4%) and 82(55.95%) genomic loci for Zhao et al.[12], and 3 lead SNPs (1.25%) and 35 genomic loci (28.68%) for Smith et al.[22].

Second, we applied the Joint Analysis of Multiple Phenotypes (JAGWAS) framework to perform a multivariate genome-wide association study (mvGWAS) in both the discovery and replication cohorts based on the single-variant GWAS result, this approach integrated the 128 UDIP-FAs' association signals for a SNP into a single summary statistic, enhancing the statistical power and thus the ability to detect novel SNPs associated with UDIP-FAs (Methods). Subsequently, we used FUMA to clump mvGWAS results based on linkage disequilibrium (LD) and to identify independent lead SNPs at each associated genomic locus (Methods). At a genome-wide significance threshold of $P = 5 \times 10^{-8}$, we identified 420 lead SNPs (LD $R^2 < 0.1$) across 300 genomic loci in the discovery cohort (Figure S2, Table S5). Among these, 182 lead SNPs (43.13%) were successfully replicated in the replication cohort ($P < 0.05/420$). In the final step, we adopted the METAL[23] and JAGWAS do the meta mvGWAS that combined the discovery cohort and replication cohort. By this way, at a genome-wide significance threshold of $P = 5 \times 10^{-8}$, we identified 939 lead SNPs (LD $R^2 < 0.1$) in 586 genomic locus regions (Figure S3, Table S6).

Comparison with previous GWAS studies

To further investigate the biological relevance of the 939 lead SNPs identified in our meta mvGWAS, we conducted association lookups in the NHGRI-EBI GWAS Catalog[24]. The results revealed that the majority (52.29%) of lead SNPs associated with UDIP-FA had not been reported in previous GWAS (Figure 3c, Table S7). Among 448 previously reported lead SNPs, 268 (59.82%) had been linked to brain MRI-derived phenotypes, including some metrics of white matter microstructure features (e.g., FA, radial diffusivity, and white matter connectome)[25-27], as well as brain morphology traits (e.g., brain shape, cortical thickness, and volume) [28,29]. Notably, SNPs in the 16q24.2 region showed strong associations with white matter microstructure (Figure 3d). In addition, 25 lead SNPs overlapped with known risk variants for several neurological disorders, including schizophrenia (SCZ)[30], Alzheimer's disease (AD)[31], and Parkinson's disease (PD)[32,33]. Six SNPs were associated with cognitive functions (e.g., general cognitive ability)[34-

[36], and 15 lead SNPs had previously been linked to educational attainment[35,37]. Interestingly, 42 of the identified lead SNPs were also associated with bone density traits (e.g., femoral neck and heel bone mineral density), particularly we observed shared colocalizations with femoral neck bone density and total body bone mineral density in the 7q31.31 region (Figure 3e, Figure S4). Apart from those, our identified SNPs also show significant association with metabolism-related traits and disease, such as High-density lipoprotein (HDL) cholesterol levels[38] and Type 2 diabetes[39].

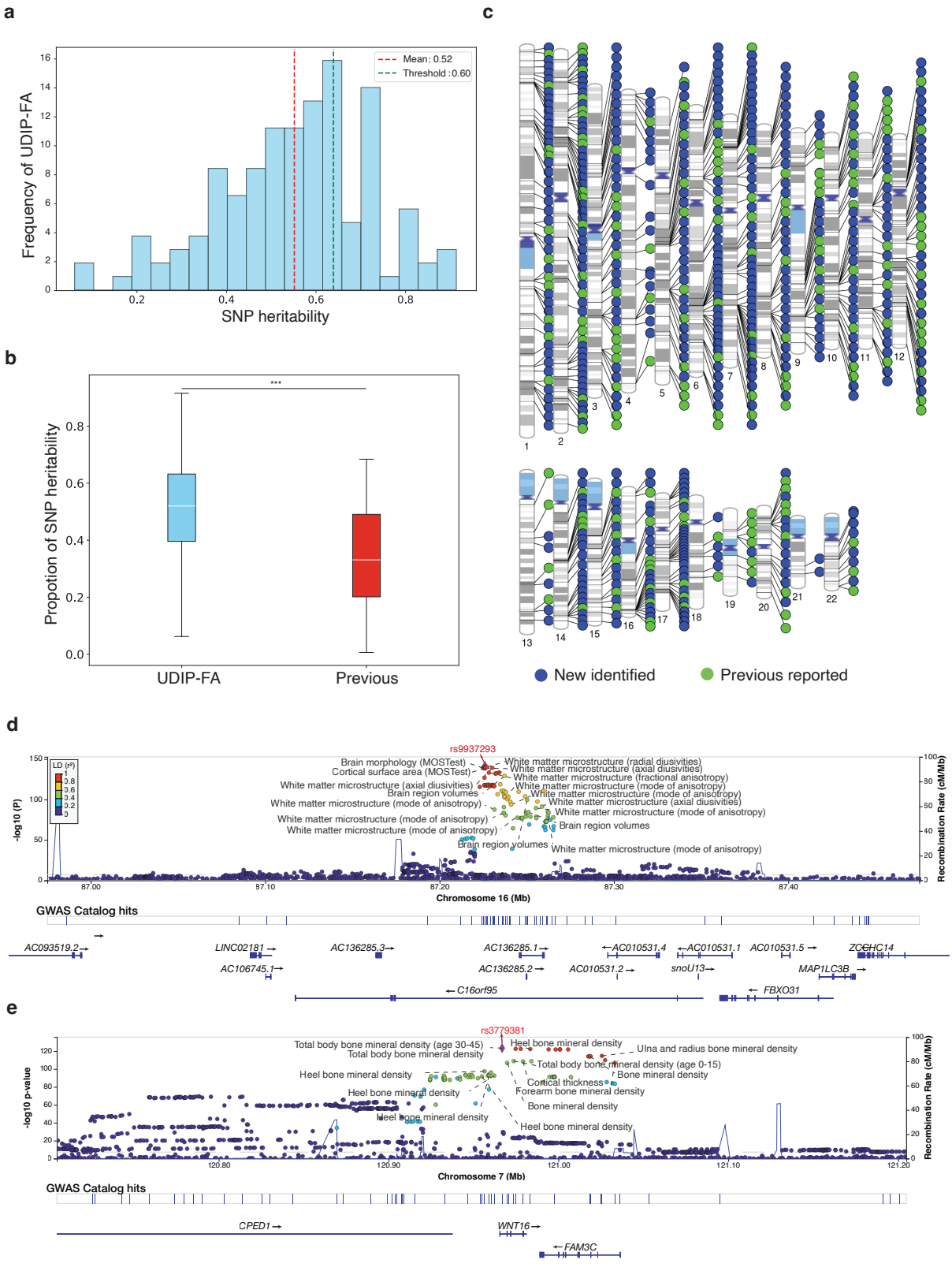

Figure: 3 SNP heritability and the associated genomic loci of UDIP-FA. (a) SNP heritability of 128 UDIP-FAs. **(b)** Comparison of SNP heritability for FA between our study and the previous study. **(c)** Identified loci by meta mvGWAS. **(d)** In 16q24.1, we observed colocalization (LD R2 $\geqslant$ 0.6) between the UDIP-FA (index variant *rs9937293*) and white matter microstructure-related features. (e) In 7q31.31, we observe colocalization between UDIP-FAs (index variant *rs379381*) and the total body BMD（total body BMD： index variant *rs380138*, Figure S4).

Gene-based association analysis and functional annotation

To explore the biological function associated with UDIP-FA, we first carried out a gene-based association analysis using MAGMA[40] on the meta mvGWAS summary statistics. This analysis identified 2,201 significant gene-level associations ($P < 0.05 / 19{,}294$) between genes and UDIP-FA (Table SX), dubbed UDIP-FA related genes (UFAGs). Among these, we replicated 126 of 413 and 56 of 137 MAGMA-identified genes from previous studies[12,25], such as *GMNC*, *MAPT*, *VCAN*, and *PTCH*. On the other hand, we also used the proximity of physical position, eQTL, chromatin interaction to map the significant SNP to genes (Table SX, Methods), we identified 2,820 UFAGs, 1,516 (53.76%) genes were replicated in MAGMA identified UFAGs (Figure S5). In the end, we identified 3,480 UFAGs, 686 genes (19.71%) show high conservation, with a probability of loss-of-function intolerance (pLI) score greater than 0.9. which indicating that a substantial proportion of these genes are under strong functional constraint.

Furthermore, we examined the phenotypic associations of the UFAGs through Topgene[41], we found that the genes associated with UDIP-FA were significantly enriched in 164 phenotypes and brain disorders. Such as white matter microarchitecture (Bonferroni-corrected $p < 6.27 \times 10^{-47}$) and brain measurements (Bonferroni-corrected $P < 4.72 \times 10^{-115}$; Figure 4b, Table SX). Some of these genes—such as *MAPT, MPP2, LAMTOR2, RERE*, *ARHGAP27*, and *SLC41A1*—were identified as risk genes for Parkinson's disease (Bonferroni-corrected $P < 1.988 \times 10^{-5}$, Table S7).

In addition, we employed MAGMA to perform gene-set enrichment analysis based on p-values from the meta mvGWAS results, evaluating 17,009 predefined functional gene sets from the MSigDB database[42]. The analysis identified 196 gene sets with significant enrichment

(Bonferroni-adjusted $P < 0.05$ for 17,009 tests; Figure 4a and Table S8). These enriched gene sets were primarily related to developmental biological processes, including "Organ Morphogenesis" (Bonferroni-adjusted $P = 7.16 \times 10^{-13}$) and "Neurogenesis" (Bonferroni-adjusted $P = 1.17 \times 10^{-8}$). Next, we conducted a MAGMA gene property analysis using human brain gene expression data from the BrainSpan database[43], stratified by 11 life-span stages and 29 distinct age groups, to assess whether gene expression levels at specific developmental stages were associated with the strength of the correlations between genes and UDIP-FA. The results revealed that UDIP-FA-associated genes (UFAGs) were significantly enriched during the prenatal period (Figure 4c), particularly before the 21st week of gestation (Bonferroni-corrected $P < 0.05$; Figure 4d).

Given that white matter development involves dynamic changes in the abundance and types of neuronal cells, we further examined the expression of UFAGs across different cell types at adult, using single-cell RNA sequencing data derived from the PsychENCODE [44]. We found that UFAGs were significantly overexpressed in glial cell types during both prenatal and postnatal developmental stages (Figures 4e and 4f), especially in astrocytes, oligodendrocytes, and microglia (Bonferroni-corrected $P < 0.05$, Figure 4f).

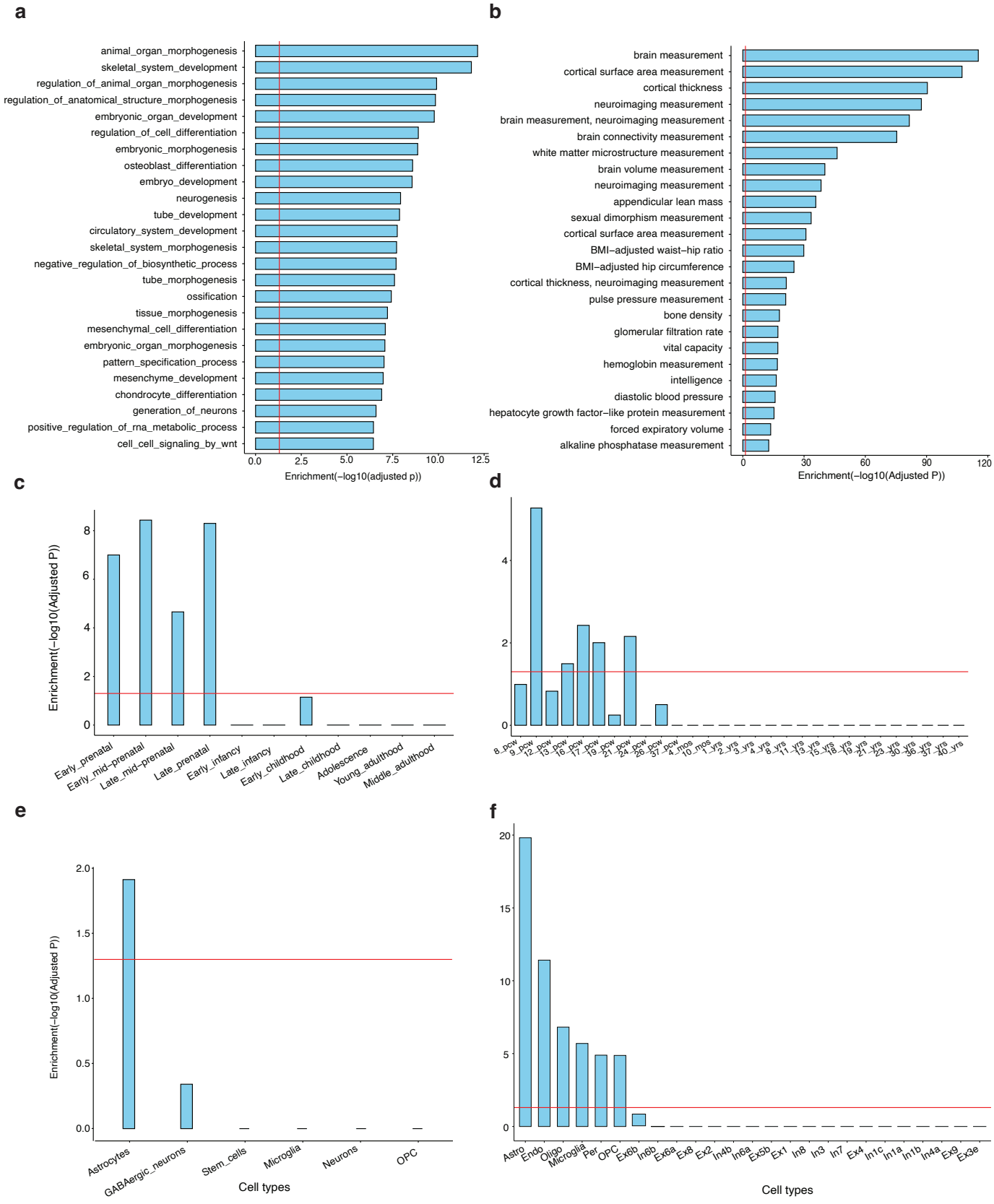

Figure 4: Functional annotation of UDIP-FA. (a) Top 25 significantly enriched Gene Ontology (GO) biological pathways. **(b)** Top 25 significantly enriched phenotypes associated with UFAGs. **(c)** and **(d)**UFAGs show prenatal up-regulation in the human brain based on BrainSpan data across 11 developmental stages or 29 age groups. **(e)** and **(f)** UFAGs are up-regulated in glial cell types based on single-cell gene expression data from the prenatal (e) and adult (f) human brain, with particularly strong expression in astrocytes. Red lines indicate the Bonferroni-corrected significance threshold of $P < 0.05$ within each analysis. PCW, postconceptional weeks. Astro, Astrocyte; Endo, Endothelial cell; Microglia, Microglial cell; Per, Pericyte; OPC, Oligodendrocyte precursor cell; Oligo, Oligodendrocyte; Ex6a, Ex6b, Ex6b Ex3e, Excitatory neuron subtypes from cortical layer 6, layer 5, and layer 5; Ex4, Ex2, Ex8, Ex1, Excitatory neuron from layer 4, layer 2, layer 8, and Layer 1; In1a, In1c, In1b, In4a, Inhibitory neuron subtypes from cortical layer 1 and layer 4; In3, In7, In8, Inhibitory neuron from layer 4, layer 3, layer 7 and layer 8.

UDIP-FA demonstrates significant associations with risk of brain disorders and cognitive functions

To evaluate the association between UDIP-FA and complex diseases, we first obtained GWAS summary statistics for various diseases from published result that without sample overlap with the UK Biobank dataset used in our study (Methods). We then computed the polygenic risk scores for each disease using PRS-CS [45]. To assess the associations between the 128 UDIP-FA features and polygenic risk scores (PRS) for various traits, we conducted canonical correlation analysis (CCA), adjusting for relevant covariates (Methods). Our results revealed significant associations between UDIP-FAs and several brain disorders (Figure 5a), including multiple sclerosis (MS; CCA correlation (r) = 0.111, Bonferroni-corrected $P = 2.95\times10^{-5}$, F test), schizophrenia (SCZ; r = 0.110, Bonferroni-corrected $P = 6.06\times10^{-5}$, F test), and amyotrophic lateral sclerosis (ALS; r = 0.104, Bonferroni-corrected $P = 3.77\times 10^{-3}$, F test). Additionally, UDIP-FAs were strongly associated with bone density–related phenotypes, such as total body bone mineral density (BMD; r = 0.332,

Bonferroni-corrected P = 2.12×10^{-307}, F test) and heel BMD (r = 0.156, Bonferroni-corrected P = 7.38×10^{-33}, F test).

To further assess the relationship between FA and cognitive functioning, we extracted fields from the UKB that were relevant to cognitive functioning. Then we examine the association between the UDIP-FA and some cognitive function used the CCA model (Methods). We found the UDIP-FA showed a significant association with fluid intelligence (r = 0.200, P=1.11×10^{-16})and reaction time (r = 0.134, P=2.220×10^{-15}). These findings are consistent with previous studies reporting associations between BMD, brain structure, and cognitive function[46], suggesting that BMD may influence white matter microstructure as reflected in FA, which in turn may relate to cognitive function.

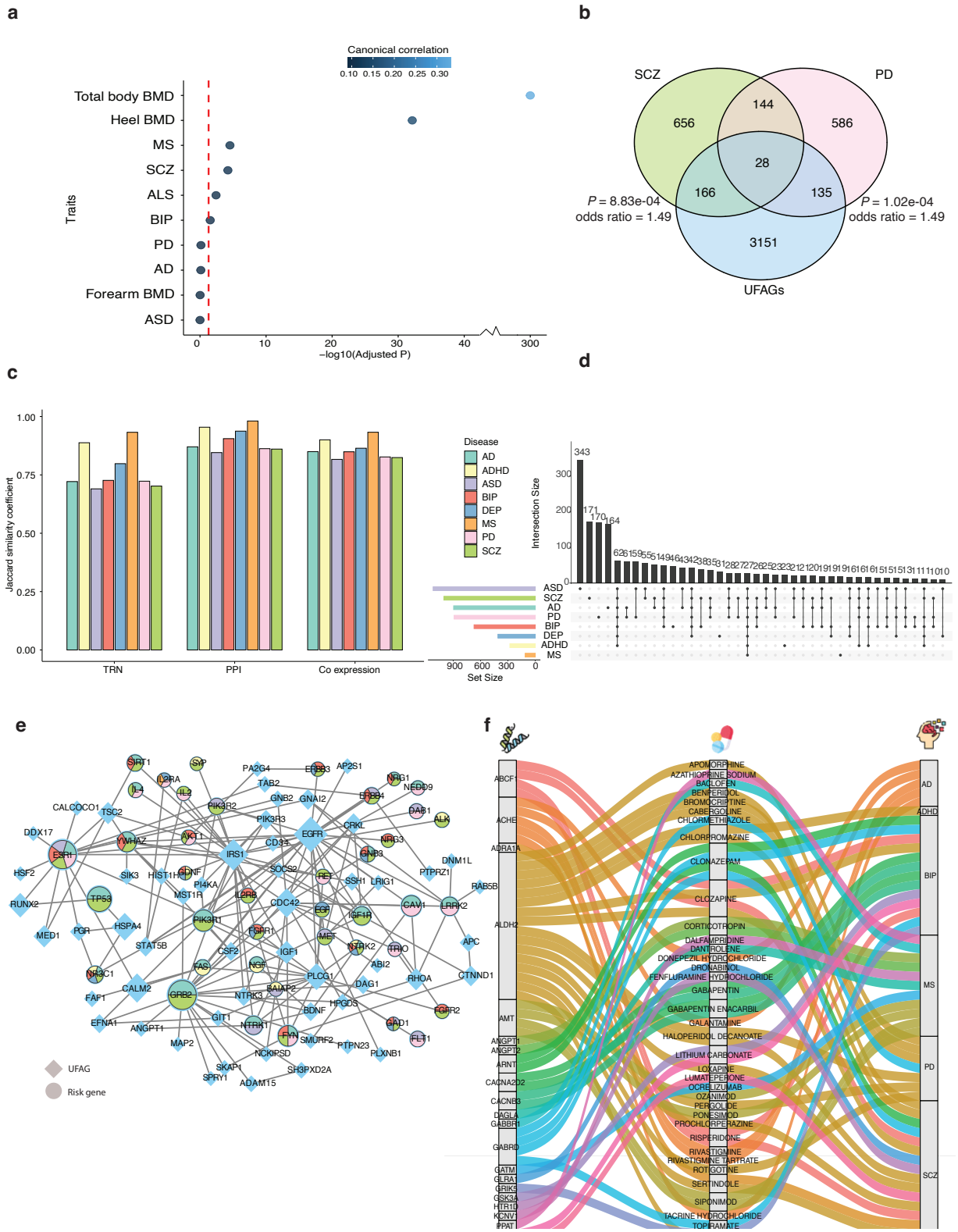

Figure 5: Associations between UDIP-FA and various diseases at both phenotypic and molecular levels. (a) Bubble plot showing significant associations between UDIP-FA and the polygenic risk scores (PRS) of brain disorders, as well as bone mineral density (BMD). Red lines indicate the Bonferroni-corrected significance threshold ($P < 0.05$) within each analysis. **(b)** Venn diagram illustrating significant enrichment of UFAGs within the risk gene sets of schizophrenia (SCZ) and Parkinson's disease (PD). *P*-values are Bonferroni-corrected. **(c)** Enrichment of UFAGs with risk genes for various brain disorders within molecular networks. Enrichment is quantified using the Jaccard distance index, where higher values indicate greater similarity. Analyses are based on transcriptional regulatory networks (TRNs), protein–protein interaction (PPI) networks, and gene co-expression networks derived from the human brain (Methods). **(d)** Overlap of protein interacting with UFAGs in brain-active PPI networks for multiple brain disorders. **(e)** Network visualization of pivotal hub modules for UFAGs in the PPI network. Diamonds represent UFAGs, circles denote disease risk genes, and pie chart colors indicate gene overlap across different brain disorders. **(f)** Tripartite network connecting subset of UFAGs, drug compounds, and brain disorders. This alluvial plot depicts associations among UFAGs (left), drug compounds (middle), and major neuropsychiatric and neurodegenerative disorders (right). Colored flows represent known gene–drug–disease relationships curated from established databases (Methods). AD, Alzheimer's disease; ADHD, Attention Deficit Hyperactivity Disorder; BIP, Bipolar Disorder; DEP, Depression; MS, Multiple Sclerosis; PD, Parkinson's Disease; SCZ, Schizophrenia; ASD, Autism Spectrum Disorders.

Genetic pleiotropy of UFAGs and risk genes in various brain disorders

Since UDIP-FA shows significant associations with various brain diseases and demonstrates potential for disease classification, we sought to investigate the underlying molecular mechanisms between WM variations captured by UDIP-FA and brain disorders. To this end, we collected eight risk gene sets associated with different brain disorders (Methods) and examined their overlap with UFAGs. Our analysis revealed that UFAGs intersect with multiple disease-associated gene sets and show particularly significant enrichment for risk genes of SCZ (Bonferroni-corrected P = 8.83

$\times 10^{-4}$, Fisher's exact test) and PD (Bonferroni-corrected $P = 1.02 \times 10^{-4}$, Fisher's exact test) (Figure 5b).

To further explore potential biological relationships between UFAGs and disease-associated genes, we analyzed interactions between UFAGs and the six risk gene sets across three brain-specific molecular network models (Methods, Table S9), we found UFAGs exhibit stronger enrichment with risk genes in protein-protein interaction (PPI, Jaccard $r = 0.90 \pm 0.05$) and co-expression networks (Jaccard $r = 0.85 \pm 0.04$) compared to transcriptional regulatory networks (TRNs, Jaccard $r = 0.77 \pm 0.09$, Figure 5c). This likely reflects their primary roles of UFAGs as structural or effector genes—such as those involved in myelination, axonal guidance, or cytoskeletal organization—rather than upstream transcriptional regulators. Several UFAGs, including *MOG, MOBP, SOX10,* and *RTN4*, are well-established contributors to oligodendrocyte development, axon guidance, and myelination. These genes demonstrate strong connectivity in protein-protein interaction and co-expression networks, underscoring their roles in white matter biology, while being less prominent in transcriptional regulatory hierarchies[43].

To investigate the impact of UFAGs on various brain disorders, we first assessed the pleiotropy of disorder-associated risk genes modulated by UFAGs within the brain-activated protein–protein interaction (PPI) network. Our analysis revealed that 55.82% of these risk genes interacting with UFAGs were implicated in at least two brain disorders (Figure 5d). Intriguingly, we identified *EGFR* as a major hub module (ranked by degree, Figure 5e), interacting with numerous neurodegenerative disease risk genes. Proteins associated with *EGFR* are significantly enriched in RTK signaling pathways, which have been directly implicated in the regulation of fractional anisotropy (FA): RTK signaling promotes oligodendrocyte precursor cell (OPC) proliferation and differentiation, and its disruption impairs myelination and reduces FA, as demonstrated in both genetic and pharmacological models [47,48].

We further examined the interactions between UFAGs and disorder-related risk genes within the human brain's co-expression and TRN networks. Consistent with the brain PPI network findings, 76.81% and 48.22% of the risk genes interacting with UFAGs were associated with at least two brain disorders in the co-expression and TRN networks, respectively (Figures S6 and S10).

To identify potential therapeutic targets, we queried the Drug–Gene Interaction Database (DGIdb) to extract stable associations between UFAGs and approved drugs (Methods), focusing

specifically on brain-related disorders. This analysis revealed that 44 UFAGs interact with 87 drugs used to treat 55 distinct brain-related diseases (Table S11). We further examined the connections between UFAGs and the eight brain disorders incorporated in our network analysis (Figure 5f) and found that many UFAGs serve as known drug targets. For example, *ACHE* is a target of anticholinesterase inhibitors such as galantamine and rivastigmine, which are well-established treatments for Alzheimer's disease. Similarly, *ALDH2* is targeted by antipsychotic drugs, including clozapine and haloperidol decanoate, both of which are used in the treatment of schizophrenia and Parkinson's disease. These findings highlight a subset of potentially druggable UFAGs and underscore shared pharmacogenomic targets across multiple brain disorders.

Comparison of UDIPs across different brain imaging modalities

Brain images acquired through different modalities provide complementary insights[49]; however, the interrelationships among these modalities remain inadequately characterized. To investigate these relationships, we conducted a comprehensive extraction and analysis of whole-brain images from three modalities—UDP-FA, UDP-T1, and UDP-T2—using data from the UKB. Cross-modality relationships were evaluated using CCA applied to 128-dimensional UDIP representations (Figure 6, Methods). Results showed that FA (0.34 ± 0.06) were heritable than T1(0.26 ± 0.03) and T2(0.25 ± 0.04) that evaluated by LDSC[14]. T1 and T2 shared the highest mutual explainability (CCA explained variance: 91%), whereas T1 was better explained by FA (74%) than T2 (69%). Building upon our prior investigation into the genetic architecture of UDP-T1 and UDP-T2, we extended the analysis to genetic correlation across all three modalities (Methods). The genetic correlation between T1 and T2 was stronger than either's relationship with FA. Furthermore, loci identified across different models revealed a consistent pattern: T1 and FA shared 374 loci (80.09% overlap), while T2 shared 399 loci (86.18%) with the same set.

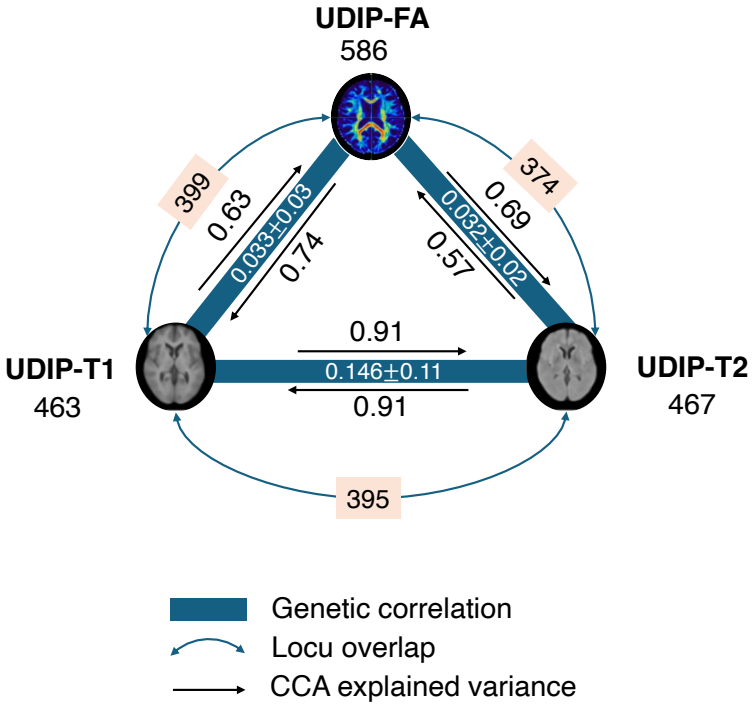

Figure 6: Cross-modality relationships among diffusion, T1-weight, and T2-weight MRI. The number below each modality label denotes the number of genome-wide significant loci identified in the multivariate GWAS. Blue solid lines represent genetic correlations estimated between each modality pair; the corresponding values are indicated alongside the lines. Black curved arrows denote canonical correlation analysis (CCA)–based explained variance between modality-specific UDIP representations. Dashed gray arrows indicate the number and proportion of overlapping loci between modality pairs.

Discussion

In this study, we developed UDIP-FA, an unsupervised deep representation of white matter (WM) microstructure and demonstrated its effectiveness in capturing biologically and genetically meaningful brain variation. UDIP-FA outperforms traditional FA phenotypes in representing population-level WM architecture, with strong predictive power for age, sex, and multiple brain disorders. UDIP-FA traits show high heritability and GWAS of UDIP-FA identified many novel

and replicable loci. The associated genes (UFAGs) are enriched for neurodevelopmental and show significant overexpression in glial cells. We further found that UFAGs are pleiotropic, overlap significantly with brain disorder risk genes, and interact with known drug targets, supporting their translational potential. UDIP-FA offers a robust and interpretable framework to advance our understanding of WM biology and its role in brain health and disease.

Compared with conventional FA phenotypes derived by hand-crafted ROI or tract-based approaches, UDIP-FA—extracted via an unsupervised 3D convolutional autoencoder—better encodes inter-regional white matter relationships, as it directly uses FA images as input, and passes them through a minimal encoder–decoder bottleneck. This design ensures maximal information compression while preserving WM-relevant patterns. We demonstrate that UDIP-FA supports higher-accuracy brain age prediction using only simple machine learning models than before[16]. Furthermore, although our network was never trained on disease labels, UDIP-FA naturally highlights disease-critical white matter tracts, such as those implicated in AD (e.g., cingulum, corpus callosum), and shows significant correlations with cognitive scores and genetic risk factors for multiple brain disorders. This finding aligns with studies showing that unsupervised learned representations can uncover subtle pathology-driven patterns and correlate with established AD biomarkers[50]. Our findings indicate that UDIP-FA serves as a robust and unbiased biomarker, capturing rich microstructural and network-level features crucial for assessing white matter integrity across ageing and disease. These representations can augment conventional image-derived phenotypes in GWAS and clinical prediction, ultimately improving both interpretability and biomarker sensitivity in neurodegenerative research.

Multi-stage GWAS of UDIP-FA have identified many novel loci that reveal the genes relevant to the biological process of myelination and glial cell function associated with WM microstructure. *rs4239889* (near *SOX10*), *SOX10* is a master regulator of oligodendrocyte differentiation, driving myelin gene expression and ensuring oligodendrocyte survival[51,52]. *rs1768234* (near *MOBP*), *MOBP* encodes a structural component of compact CNS myelin, marking mature oligodendrocyte functionality, and it plays a crucial role in myelination and axonal integrity that influencing white matter microstructure. *rs34580448* (near *VCAN*), *rs11259505* (regulated the *ADAMTSL4* by eQTL), *VCAN, and ADAMTSL4* are extracellular matrix-related genes that regulate pericellular

and microfibrillar scaffolding, respectively, contributing to axonal stability and myelination processes that underlie white matter microstructural integrity[10,53]. Additionally, some UIDP-FA related loci that are members of the WNT gene family, such as WNT3A, WNT5A acting through canonical Wnt/β-catenin signaling, are essential regulators of white matter myelination, with dysregulated pathway activity in oligodendrocyte precursor cells shown to delay developmental myelination and remyelination in the CNS[54]. Additionally, WNT16, along with WNT4 and WNT5A, are strongly implicated in bone mineral density (BMD) and skeletal strength, supported by GWAS and functional studies linking WNT16 to cortical thickness, fracture risk, and osteoblast differentiation[55]. These findings suggest that Wnt signaling may represent a shared molecular mechanism underlying both white matter integrity and BMD, potentially linking neurodevelopmental and skeletal pathways through common genetic regulation.

UFAGs characterize the potential underlying molecular regulation of white matter in different brain diseases and have the potential to be a drug target. In the brain TRN, our findings suggest that the transcription factor *MEF2C* plays a central role in the shared genetic architecture between white matter integrity and major psychiatric disorders[56]. Specifically, we show that MEF2C regulates multiple pleiotropic risk genes implicated in both BIP and SCZ, such as *GRIN2A*, *MCHR2*, and *YWAH*. These genes are involved in synaptic signaling, neurotransmitter regulation, and intracellular signaling pathways that are essential for neurodevelopment and cognitive function. For example, *GRIN2A* encodes an NMDA receptor subunit critical for synaptic plasticity and has been linked to SCZ and cognitive dysfunction[57]. Given that *MEF2C* functions as a transcription factor involved in the regulation of synaptic and neurodevelopmental genes[58], it is plausible that its regulatory influence extends to pleiotropic risk genes such as *GRIN2A*, *MCHR2*, and *YWAH*, which are implicated in BIP and SCZ. In addition, the UFAG, ANGPT1, serves as a convergent downstream target of multiple risk transcription factors implicated in distinct brain disorders. Notably, in the context of MS, *ANGPT1* is regulated by key immune-modulatory TFs such as *PPARG* and *STAT3*, where PPARG mediates anti-inflammatory responses and ameliorates disease progression, while *STAT3* promotes pro-inflammatory Th17 differentiation and neuroinflammation[59]. Functionally, *ANGPT1* plays a critical role in maintaining blood-brain barrier (BBB) integrity and vascular stabilization, and its dysregulation has been implicated in BBB breakdown and increased neurovascular permeability observed in MS lesions[60], We also

found that it interacts with the MS treatment drug corticotropin, which suggests that *ANGPT1* may serve as a potential therapeutic mediator or downstream effector in modulating vascular responses during immunomodulatory treatment in MS.

Our findings delineate a hierarchy of modality integration across brain imaging and genetics: T1 and T2 modalities form a tightly integrated pair, both phenotypically and genetically (average cross-modality correlation and overlapping UDIP-derived loci)[14], while FA captures complementary microstructural information (e.g., voxel-wise aging effects distinct from T2 contrasts) [61]. This layered understanding has several implications. First, it recommends selecting structurally similar modalities (e.g., T1–T2) when designing imaging-genetics studies to maximize shared signal, as deep-embedding GWAS showed enhanced overlap and statistical power in these modalities. Second, discovering modality-specific loci enriches our ability to link particular genes with distinct neurobiological substrates— FA-associated loci highlight genes involved in myelination or fiber tract integrity[62], whereas T1/T2-associated loci are more likely to implicate genes involved in tissue composition, cellular organization, or iron homeostasis, reflecting their sensitivity to cell density and regional iron concentration[63,64], as reflected by loci uniquely identified from UDIP features. Lastly, these insights can refine trait mapping in neurodegenerative and developmental disorders by targeting imaging features with maximal genetic sensitivity, leveraging modality-specific genetic signals uncovered in multivariate GWAS frameworks.

We demonstrate that UDIP-FAs show strong correlations with traditional FA phenotypes, enhancing their interpretability. These patterns extend beyond predefined, single-region volumetric features such as IDPs, which presents challenges for interpretability. Although our PerDI approach offers a partial solution, further improvements are needed. Additionally, our UDIP-FA GWAS was conducted exclusively on European populations, limiting its ethnographic generalizability. Future studies will aim to validate the robustness of these findings across diverse populations.

In summary, our study is the first to apply unsupervised deep representation learning to DTI derived FA images, leading to the development of UDIP-FA. We demonstrate that UDIP-FA captures a more informative and functionally relevant representation of white matter microstructure, enabling deeper insights into its genetic architecture and disease associations. Importantly, UDIP-FA reveals previously unrecognized links between white matter integrity and

brain disorders, and highlights potential therapeutic targets, suggesting its promise as a bridge between imaging biomarkers and pharmacological intervention.

Methods

Collection and preprocessing of FA images

UK Biobank (UKB) was chosen for this study because it represents the largest publicly available brain imaging dataset, uniformly processed through standardized pipelines, ensuring consistency and comparability across subjects[65]. We used data from 30789 UKB individuals of British ancestry (self-reported ethnic background, Data-Field 21000) that have the diffusion MRI image data. The diffusion MRI data in UKBB were primarily acquired using Siemens Skyra 3T MRI scanners operating VD13A SP4, equipped with a standard Siemens 32-channel RF head coil. The diffusion-weighted images (DWIs) utilized a multi-shell diffusion sequence, optimized for consistent quality across multiple imaging centers[61]. To maximize generalizability and reduce feature engineering, we followed the straightforward preprocessing pipeline provided by the UKBB imaging team, primarily utilizing the FMRIB Software Library (FSL; https://www.fmrib.ox.ac.uk/ukbiobank/). Key preprocessing steps provided by UKBB include correction for motion and eddy current distortions using FSL's eddy tool, diffusion tensor fitting using FSL's DTIFIT, and generation of bias-field-corrected FA images[66]. Subsequently, all FA images were spatially normalized to the MNI152 space provided by UKBB via non-linear registration using FSL FNIRT. Normalization ensured the standardization of head sizes and alignment of brain structures across subjects, while preserving relevant structural deformation information. All individuals were aged between 40 and 80 years and the proportion of females was 52.7%.

Unsupervised Deep Neural Network for Representing FA image

For obtaining the UDIP-FA, we adopted our previously proposed model - Deep 3D convolutional autoencoder to obtain the 128-dimensional phenotype. A separate model was trained for FA images. The architecture was implemented using PyTorch and trained with the PyTorch Lightning

framework. To obtain representations of the whole brain, we take the full-resolution brain FA images as input. The model consisted of an initial convolutional block, four encoder blocks, a linear latent space of 128 dimensions, four decoder blocks, and a final convolutional block and has 138.12 million parameters (Figure S8) [14]. The output reconstructed image is of the same size as the input MRI (182 × 218 × 182).

Our model employs a standard convolutional autoencoder without skip connections to preserve maximal information through the bottleneck, enabling each latent vector (UDIP) to capture global brain morphology. Unlike prior approaches that reduce resolution, extract patches, or focus only on WM tracts, we process full-resolution, whole-brain MRIs, maintaining anatomical completeness. Leveraging the large UK Biobank dataset, our unsupervised framework is the first of its kind to derive comprehensive, scalable imaging phenotypes (UDIP-FA) for brain-wide GWAS.

For training this model, we randomly split the dataset into training (75%) and validation (25%) sets, using the latter to tune hyperparameters and select the best-performing model checkpoint based on validation loss. Our autoencoder uses a voxel-wise regression framework with no output activation, optimized via masked mean squared error focused solely on brain regions. Models were trained for 75 epochs using the Adam optimizer and a well-tuned learning rate, with training accelerated by seven NVIDIA A100 GPUs. This setup enabled efficient and anatomically precise image reconstruction for FA images.

Interpretation and application of UDIP-FA

To interpret spatial representations of each of the 128 UDIP-FAs, we developed PerDI—a perturbation-based approach. For a given UDIP-FA, Gaussian noise (σ) is added while other dimensions remain unchanged. The original decoder reconstructs images from the perturbed and unperturbed representations for 500 randomly selected individuals. A paired t-test between these two sets of images yields an absolute t-map highlighting brain regions associated with the target UDIP. The resulting map is smoothed with a Gaussian filter ($\sigma = 3$) to mitigate registration imperfections.

To explore the regional enrichment of UDIP-FA, we used the brain tissue segmentation atlas[67] and ICBM DTI-81 atlas[15] to annotate t-maps. Voxels were ranked by t-values in descending order. For each atlas-defined region, a normalized Kolmogorov–Smirnov (K–S) statistic was computed to quantify regional enrichment. The K–S curve is defined as $\frac{k}{V} - \frac{n}{N}$, where k is the number of voxels from a region among the top n ranked voxels, V is the number of voxels in the region, and N is the total number of voxels. The K-S value is the maximum value along the K-S curve. A higher K–S value indicates stronger representation of the region by the corresponding UDIP. These spatial enrichments were then used to associate UDIP-specific brain regions with brain disorders.

UDIP for predicting disease status and associated with cognitive function

To get the disease status of the UKB samples, we using the ICD-10 code to obtain the patients for different brain disorders, include AD (F00, G30), PD (G20), SCZ(F20), DEP(F32) and MS(G35). And obtain the cognitive function of the fluid intelligence score (data field: 20016), prospective memory (data field: 20018), mean time to correctly identify matches (20023).

To evaluate the classification performance of UDIP-FA features across various brain disorders under imbalanced sample conditions (e.g., 26,000 controls vs. 216 MS cases), we adopted a five-fold stratified cross-validation framework combined with stochastic downsampling of the majority class. Specifically, for each cross-validation fold, the dataset was split into training and testing sets while preserving the original class distribution using stratified sampling.

Within each training set, we randomly downsampled the majority class (controls) to match the number of minority class samples (e.g., MS cases), ensuring class balance during model training. Formally, given two classes A and B, where |A| > |B|, a random subset $A' \subset A$ was sampled such that |A'| = |B|, and the balanced training data consisted of $A' \cup B$. The held-out testing fold was kept at its original class distribution to fairly assess model generalization.

For the classification task, we employed gradient boosted decision trees (GBDT) implemented using the LightGBM Python package with default hyperparameters. Model performance was evaluated on each test fold using the area under the receiver operating characteristic curve (AUC),

and the mean AUC across the five folds was reported. Feature importance was determined using LightGBM's gain-based ranking, averaged across folds to identify robust predictive markers.

Genetic data preprocessing and association analysis

Genetic analyses were performed on individuals from the UKB with European ancestry, who also had genotypes and diffusion MRI image data. Standard quality control procedures were then applied to the UKB v3 imputed genetic data[68]. These procedures included the following steps: (1) exclusion of individuals with failed genotyping, abnormal heterozygosity status, or withdrawn consents; (2) removal of participants genetically related—up to the third degree—to another participant, as inferred by kinship coefficients implemented in PLINK[69]; (3) elimination of variants with a minor allele frequency below 0.01%; (4) removal of variants with a genotype missing rate exceeding 10%; (5) exclusion of variants failing the Hardy-Weinberg equilibrium test at the 1e-07 level; 6) elimination of variants with an imputation INFO score below 0.8. Post quality control, we retained 30,789 individuals and 8,931,083 variants.

For genome-wide association analysis (GWAS) of the UDIP-FA, we adopt the multiple-stage GWAS analysis for the UDIP-FA (Figure S9). 1) We first divided the samples into discovery and replication cohorts, followed by conducting a genome-wide association study (GWAS) on the 128-dimensional UDIP traits separately for each cohort using mixed linear models implemented in GCTA. Covariates included age (field ID 21003), age squared, sex (field ID 31), interaction terms (sex × age, sex × age^2), the first 10 genetic principal components (field ID 22009), head size (field ID 25000), head position in the scanner (field IDs 25756–25758), scanner table position (field ID 25759), assessment center location (field ID 54), and date of assessment (field ID 53).To evaluate the stability of the GWAS results, we conducted LD score regression (LDSC) for the whole GWAS, which yielded intercept values close to 1, indicating that the observed inflation in test statistics is likely due to polygenicity rather than confounding factors. We also validated the reliability of our findings by comparing results between the discovery and replication cohorts. 2). To assess whether single genetic variants influence multiple UDIP dimensions, we employed JAGWAS[70] to perform multivariate GWAS analyses in both the discovery and replication cohorts. 3) We used the method METAL[23] to perform the meta-analysis to integrate discovery and replication cohort of 128 GWAS of UDIP-FA to improve the detection effectiveness of our SNPs. 4) Finally, we applied the JAGWAS[70] to perform the multivariate GWAS analysis on 128 meta GWAS summary statistic,

this method to integrate the 128 meta GWAS of UDIP into a single multivariate GWAS summary statistic.

The *P*-value threshold for selecting the significant multivariate GWAS tag variants is 5e-08.

Prioritizing UFAG-associated genes and gene expression analysis

In the study of the UDIP-FA meta mvGWAS, MAGMA (version 1.08)[40] was used to perform a gene-based association analysis for 19,218 protein-coding genes. The default MAGMA parameter settings were applied, with a zero-window size around each gene. Subsequently, FUMA functional annotation and mapping analysis were performed, which involved annotating variants with their biological functionality and linking them to candidate target genes through a combination of eQTL and 3D chromatin interaction mappings. Brain-related tissues/cells were selected for all options, and default parameters were used.

In addition, to explore the tissue/cell specific and developmental stage using the MAGMA based on tissue expression data and cell expression data. We used MAGMA to test whether cell or tissue-specific gene expression levels predict the strength of GWAS associations for UDIP-FAs. This gene-property analysis assesses continuous gene characteristics (e.g., expression in a specific tissue) rather than predefined gene sets. After performing gene-level association analysis, each gene's p-value (p_g) was converted to a Z-score:

$$Z_g = \Phi^{-1}(1 - p_g)$$

where Φ^{-1} is the probit (inverse normal) function. We then modeled Z_g via linear regression:

$$Z_g = \beta_0 + \beta_1 E_{t,g} + \beta_2 A_g + \beta_3 C_g + \varepsilon_g$$

Where $E_{t,g}$ is expression level of gene g in tissue t, A_g was average expression across all tissues (controls for baseline), C_g is covariates (e.g., gene size, SNP density); β_1 was the coefficient testing whether tissue t expression is positively associated with gene-level association.

A significantly positive β_1 indicates that higher expression in tissue t is associated with stronger genetic effects.

For tissue and cell type expression data, we used BrainSpan[43] and PsychENCODE [44]. We applied Bonferroni correction across all tested tissue or cell types.

Computing polygenic scores and correlation with UDIP-FA

The polygenic score (PGS) represents an estimate of an individual's genetic risk for a given trait. To estimate the association between UDIP-FA and genetic risk for different traits, the polygenic score for complex traits was generated using PRS-CS[45] by default parameters, which based on genetic data of Europeans from UKB with the collected GWAS data for 11 complex traits (Table S12), including SCZ, BIP, ASD, ALS, AD, PD, Epilepsy, MS, total body BMD, femoral BMD, and Heel BMD. These GWAS studies do not overlap in sample composition with the UKB cohort used for UDIP-FA in our analysis.

Numerous polygenic profiles of complex traits were generated for each trait using PLINK[69] based on the output of PRS-CS. To evaluate the association between the polygenic risk scores (PRS) of various traits and UDIP-FA, we applied canonical correlation analysis (CCA), adjusting for covariates used in the GWAS, including age, sex, the first 10 genetic principal components, head size, head position in the scanner, scanner table position, assessment center location, and date of assessment. All *P*-values were derived from *F*-tests and corrected for multiple comparisons using the Bonferroni correction.

Collection of risk gene for brain disorders

Risk genes associated with brain disorders were compiled from various resources: (1) risk genes of ADHD were sourced from the ADHDgene database (http://adhd.psych.ac.cn), selecting only those with support from at least 60% of all studies included in the database[71]; (2) risk genes of ASD were downloaded from the AutDB database (http://autism.mindspec.org/autdb) and were supplemented with risk genes from recent studies[72,73]; (3) risk genes of SCZ were obtained from the SZGene database (http://www.szgene.org/) and from research by Wang *et al.*[44,74]; (4) risk genes of BIP were gathered from DisGeNet[75]; (5) risk genes of MDD were downloaded from the Polygenic Pathways database (http://www.polygenicpathways.co.uk/depression.htm); (6) risk genes of AD were obtained from the ALzGene database (http://www.alzgene.org)[76]; (7) risk genes of PD were obtained from the PDGene database (http://www.pdgene.org)[77]. (8) risk genes of MS from the DisGeNET (v25.1.1, https://disgenet.com/)[78].The full list of these risk genes can be found in Table SX.

Collection of molecular networks and drug interaction networks

Three extensive molecular networks were utilized in this study to investigate the association between UFAGs and brain disorders: (1) Brain-specific TRNs were obtained from Pearl *et al.*[79], which included 741 transcription factors (TFs) and 11,092 target genes; (2) Brain-active PPI networks were reconstructed by first downloading the global PPI networks from STRING (https://string-db.org), followed by retaining of protein pairs with physical interaction scores over 700, and proteins active in the adult human brain[80] (expression value > 0), which finally included 8,568 proteins and 114,892 interaction edges (Table S13); (3) Gene co-expression networks in adult brain were generated by first removing lowly expressed genes (expression value < 0.3) and then retaining top 500,000 significant co-expression pairs between genes (*FDR* < 0.01, Pearson correlation test) using gene expression data from adult human brain[80].

To construct a high-confidence gene–drug target interaction network, we retrieved drug–gene interaction data from the Drug–Gene Interaction Database (DGIdb, version 5.09)[81]. To ensure biological relevance and clinical applicability, we applied the following stringent filtering criteria: (1) only interactions involving approved drugs were retained; (2) drugs annotated as immunotherapies or anti-neoplastic agents were excluded to focus on agents with broader

therapeutic profiles; (3) we restricted interactions to those annotated with direct and well-defined mechanisms, such as inhibitor, agonist, antagonist, activator, blocker, or binder; and The resulting gene–drug target network, where edges indicate reliable, mechanism-defined drug–gene interactions suitable for downstream biological and therapeutic analysis.

Network analysis and visualization

To uncover disorder-specific topologies associated with UFAG, subnetworks corresponding to each disorder and UDIP-FA were extracted using the criterion that one side of the edge is a disorder risk gene or UFAG. The maximal connectivity subgraph was then extracted as the disorder-specific topology. To estimate the correlation of two sub-networks, such as a UFAG-associated sub-network and an PD-related sub-network, the Jaccard distance was employed to measure the enrichment between the networks, defined as follows:

$$J(A, B) = \frac{A \cap B}{A \cup B}$$

where A was the node set of UFAG-associated sub-network, B was the node set of PD-related sub-network.

For better visualization, we created nodes for each UFAG and other risk genes, connecting all nodes via protein-protein interaction or transcriptional regulation. Finally, we arranged the networks using a perfuse circle layout. In the figure, we only presented the UFAG-associated subnetwork. Network visualization was performed using Cytoscape[82].

Correlation analysis between UDIP-FA, UDIP-T1 and UDIP-T2

To evaluate the shared information between 128-dimensional UDIP-FA and UDIPs of other modality (T1-weight MRI, UDIP-T1; T2-weight MRI, UDIP-T2), we first performed canonical correlation analysis (CCA). Our implementation is based on singular value decomposition (SVD). Given two matrices of different type UDIP, X and Y, we compute their SVD as:

$$X = U_1 S_1 V_1^T, \quad Y = U_2 S_2 V_2^T$$

We then calculate the SVD of the inner product $U_1^T U_2 = USV^T$ to obtain the canonical correlations S. To quantify how much variance of one space can be explained by the other, we define the variance of X explained by Y and vice versa as follows:

$$\mathrm{Var}(X \leftarrow Y) = \frac{|S_1 U \circ S|_F^2}{|S_1|_F^2}, \quad \mathrm{Var}(Y \leftarrow X) = \frac{|S_2 V \circ S|_F^2}{|S_2|_F^2}$$

where $\circ$ denotes element-wise multiplication, and $|\cdot|_F$ is the Frobenius norm. This formulation reflects the amount of signal preserved across latent representations of different dimensionalities.

To estimate the genetic level association between T1, T2, and FA, we then adopted LDSC to calculate genetic correlation and using the R language to get the loci overlap.

Data availability

The entire GWAS summary statistics dataset will be uploaded to the GWAS catalog later.

Code availability

The codes for this study can be found at https://github.com/Soulnature/FA_endo

Ethics declarations

Our analysis was approved by UTHealth committee for the protection of human subjects under No. HSC-SBMI-20-1323. UKBB has secured informed consent from the participants in the use of their data for approved research projects. UKBB data was accessed via approved project 24247.

Acknowledgements

This work was partly supported by grants from the National Institute on Aging U01AG070112 and R01AG081398.

Competing interest

The authors declare that they have no competing interests.

References

1 Groh, J. & Simons, M. White matter aging and its impact on brain function. *Neuron* **113**, 127-139 (2025). https://doi.org/10.1016/j.neuron.2024.10.019

2 Thomason, M. E. & Thompson, P. M. Diffusion imaging, white matter, and psychopathology. *Annu Rev Clin Psychol* **7**, 63-85 (2011). https://doi.org/10.1146/annurev-clinpsy-032210-104507

3 Penke, L. *et al.* White matter integrity in the splenium of the corpus callosum is related to successful cognitive aging and partly mediates the protective effect of an ancestral polymorphism in ADRB2. *Behav Genet* **40**, 146-156 (2010). https://doi.org/10.1007/s10519-009-9318-4

4 Penke, L. *et al.* A general factor of brain white matter integrity predicts information processing speed in healthy older people. *J Neurosci* **30**, 7569-7574 (2010). https://doi.org/10.1523/JNEUROSCI.1553-10.2010

5 Barysheva, M., Jahanshad, N., Foland-Ross, L., Altshuler, L. L. & Thompson, P. M. White matter microstructural abnormalities in bipolar disorder: A whole brain diffusion tensor imaging study. *Neuroimage Clin* **2**, 558-568 (2013). https://doi.org/10.1016/j.nicl.2013.03.016

6 Carballedo, A. *et al.* Reduced fractional anisotropy in the uncinate fasciculus in patients with major depression carrying the met-allele of the Val66Met brain-derived neurotrophic factor genotype. *Am J Med Genet B Neuropsychiatr Genet* **159B**, 537-548 (2012). https://doi.org/10.1002/ajmg.b.32060

7 Mandl, R. C. *et al.* Altered white matter connectivity in never-medicated patients with schizophrenia. *Hum Brain Mapp* **34**, 2353-2365 (2013). https://doi.org/10.1002/hbm.22075

8 Sprooten, E. *et al.* White matter integrity in individuals at high genetic risk of bipolar disorder. *Biol Psychiatry* **70**, 350-356 (2011). https://doi.org/10.1016/j.biopsych.2011.01.021

9 Kochunov, P. *et al.* Heritability of fractional anisotropy in human white matter: a comparison of Human Connectome Project and ENIGMA-DTI data. *Neuroimage* **111**, 300-311 (2015). https://doi.org/10.1016/j.neuroimage.2015.02.050

10 Rutten-Jacobs, L. C. A. *et al.* Genetic Study of White Matter Integrity in UK Biobank (N=8448) and the Overlap With Stroke, Depression, and Dementia. *Stroke* **49**, 1340-1347 (2018). https://doi.org/10.1161/STROKEAHA.118.020811

11 Persyn, E. *et al.* Genome-wide association study of MRI markers of cerebral small vessel disease in 42,310 participants. *Nat Commun* **11**, 2175 (2020). https://doi.org/10.1038/s41467-020-15932-3

12 Zhao, B. *et al.* Common genetic variation influencing human white matter microstructure. *Science* **372** (2021). https://doi.org/10.1126/science.abf3736

13 McInnes, L., Healy, J. & Melville, J. Umap: Uniform manifold approximation and projection for dimension reduction. *arXiv preprint arXiv:1802.03426* (2018).

14 Patel, K. *et al.* Unsupervised deep representation learning enables phenotype discovery for genetic association studies of brain imaging. *Commun Biol* **7**, 414 (2024). https://doi.org/10.1038/s42003-024-06096-7

15 Mori, S. *et al.* Stereotaxic white matter atlas based on diffusion tensor imaging in an ICBM template. *Neuroimage* **40**, 570-582 (2008). https://doi.org/10.1016/j.neuroimage.2007.12.035

16 Gao, C. *et al.* Predicting Age from White Matter Diffusivity with Residual Learning. *ArXiv* (2024).

17 Gozdas, E. *et al.* Focal white matter disruptions along the cingulum tract explain cognitive decline in amnestic mild cognitive impairment (aMCI). *Sci Rep* **10**, 10213 (2020). https://doi.org/10.1038/s41598-020-66796-y

18 Delvenne, J. F., Scally, B. & Rose Burke, M. Splenium tract projections of the corpus callosum to the parietal cortex classifies Alzheimer's disease and mild cognitive impairment. *Neurosci Lett* **810**, 137331 (2023). https://doi.org/10.1016/j.neulet.2023.137331

19 Welton, T., Kent, D., Constantinescu, C. S., Auer, D. P. & Dineen, R. A. Functionally relevant white matter degradation in multiple sclerosis: a tract-based spatial meta-analysis. *Radiology* **275**, 89-96 (2015). https://doi.org/10.1148/radiol.14140925

20 Diehl, B. *et al.* Abnormalities in diffusion tensor imaging of the uncinate fasciculus relate to reduced memory in temporal lobe epilepsy. *Epilepsia* **49**, 1409-1418 (2008). https://doi.org/10.1111/j.1528-1167.2008.01596.x

21 Bulik-Sullivan, B. *et al.* An atlas of genetic correlations across human diseases and traits. *Nat Genet* **47**, 1236-1241 (2015). https://doi.org/10.1038/ng.3406

22 Smith, S. M. *et al.* An expanded set of genome-wide association studies of brain imaging phenotypes in UK Biobank. *Nat Neurosci* **24**, 737-745 (2021). https://doi.org/10.1038/s41593-021-00826-4

23 Willer, C. J., Li, Y. & Abecasis, G. R. METAL: fast and efficient meta-analysis of genomewide association scans. *Bioinformatics* **26**, 2190-2191 (2010). https://doi.org/10.1093/bioinformatics/btq340

24 Buniello, A. *et al.* The NHGRI-EBI GWAS Catalog of published genome-wide association studies, targeted arrays and summary statistics 2019. *Nucleic Acids Res* **47**, D1005-D1012 (2019). https://doi.org/10.1093/nar/gky1120

25 Zhao, B. *et al.* Large-scale GWAS reveals genetic architecture of brain white matter microstructure and genetic overlap with cognitive and mental health traits (n = 17,706). *Mol Psychiatry* **26**, 3943-3955 (2021). https://doi.org/10.1038/s41380-019-0569-z

26 Sha, Z., Schijven, D., Fisher, S. E. & Francks, C. Genetic architecture of the white matter connectome of the human brain. *Sci Adv* **9**, eadd2870 (2023). https://doi.org/10.1126/sciadv.add2870

27 Fan, C. C. *et al.* Multivariate genome-wide association study on tissue-sensitive diffusion metrics highlights pathways that shape the human brain. *Nat Commun* **13**, 2423 (2022). https://doi.org/10.1038/s41467-022-30110-3

28 van der Meer, D. *et al.* Boosting Schizophrenia Genetics by Utilizing Genetic Overlap With Brain Morphology. *Biol Psychiatry* **92**, 291-298 (2022). https://doi.org/10.1016/j.biopsych.2021.12.007

29 Shadrin, A. A. *et al.* Vertex-wise multivariate genome-wide association study identifies 780 unique genetic loci associated with cortical morphology. *Neuroimage* **244**, 118603 (2021). https://doi.org/10.1016/j.neuroimage.2021.118603

30 Trubetskoy, V. *et al.* Mapping genomic loci implicates genes and synaptic biology in schizophrenia. *Nature* **604**, 502-508 (2022). https://doi.org/10.1038/s41586-022-04434-5

31 Dalmasso, M. C. *et al.* The first genome-wide association study in the Argentinian and Chilean populations identifies shared genetics with Europeans in Alzheimer's disease. *Alzheimers Dement* **20**, 1298-1308 (2024). https://doi.org/10.1002/alz.13522

32 Smeland, O. B. *et al.* Genome-wide Association Analysis of Parkinson's Disease and Schizophrenia Reveals Shared Genetic Architecture and Identifies Novel Risk Loci. *Biol Psychiatry* **89**, 227-235 (2021). https://doi.org/10.1016/j.biopsych.2020.01.026

33 Kim, J. J. *et al.* Multi-ancestry genome-wide association meta-analysis of Parkinson's disease. *Nat Genet* **56**, 27-36 (2024). https://doi.org/10.1038/s41588-023-01584-8

34 Davies, G. *et al.* Study of 300,486 individuals identifies 148 independent genetic loci influencing general cognitive function. *Nat Commun* **9**, 2098 (2018). https://doi.org/10.1038/s41467-018-04362-x

35 Lee, J. J. *et al.* Gene discovery and polygenic prediction from a genome-wide association study of educational attainment in 1.1 million individuals. *Nat Genet* **50**, 1112-1121 (2018). https://doi.org/10.1038/s41588-018-0147-3

36 Hindley, G. *et al.* Multivariate genetic analysis of personality and cognitive traits reveals abundant pleiotropy. *Nat Hum Behav* **7**, 1584-1600 (2023). https://doi.org/10.1038/s41562-023-01630-9

37 Okbay, A. *et al.* Polygenic prediction of educational attainment within and between families from genome-wide association analyses in 3 million individuals. *Nat Genet* **54**, 437-449 (2022). https://doi.org/10.1038/s41588-022-01016-z

38 Koskeridis, F. *et al.* Pleiotropic genetic architecture and novel loci for C-reactive protein levels. *Nat Commun* **13**, 6939 (2022). https://doi.org/10.1038/s41467-022-34688-6

39 Vujkovic, M. *et al.* Discovery of 318 new risk loci for type 2 diabetes and related vascular outcomes among 1.4 million participants in a multi-ancestry meta-analysis. *Nat Genet* **52**, 680-691 (2020). https://doi.org/10.1038/s41588-020-0637-y

40 de Leeuw, C. A., Mooij, J. M., Heskes, T. & Posthuma, D. MAGMA: generalized gene-set analysis of GWAS data. *PLoS Comput Biol* **11**, e1004219 (2015). https://doi.org/10.1371/journal.pcbi.1004219

41 Chen, J., Bardes, E. E., Aronow, B. J. & Jegga, A. G. ToppGene Suite for gene list enrichment analysis and candidate gene prioritization. *Nucleic Acids Res* **37**, W305-311 (2009). https://doi.org/10.1093/nar/gkp427

42 Liberzon, A. *et al.* Molecular signatures database (MSigDB) 3.0. *Bioinformatics* **27**, 1739-1740 (2011). https://doi.org/10.1093/bioinformatics/btr260

43 Miller, J. A. *et al.* Transcriptional landscape of the prenatal human brain. *Nature* **508**, 199-206 (2014). https://doi.org/10.1038/nature13185

44 Wang, D. *et al.* Comprehensive functional genomic resource and integrative model for the human brain. *Science* **362** (2018). https://doi.org/10.1126/science.aat8464

45 Ge, T., Chen, C. Y., Ni, Y., Feng, Y. A. & Smoller, J. W. Polygenic prediction via Bayesian regression and continuous shrinkage priors. *Nat Commun* **10**, 1776 (2019). https://doi.org/10.1038/s41467-019-09718-5

46 Stefanidou, M. *et al.* Bone Mineral Density Measurements and Association With Brain Structure and Cognitive Function: The Framingham Offspring Cohort. *Alzheimer Dis Assoc Disord* **35**, 291-297 (2021). https://doi.org/10.1097/WAD.0000000000000453

47 Rivera, A. D. *et al.* Epidermal Growth Factor Pathway in the Age-Related Decline of Oligodendrocyte Regeneration. *Front Cell Neurosci* **16**, 838007 (2022). https://doi.org/10.3389/fncel.2022.838007

48 Scafidi, J. *et al.* Intranasal epidermal growth factor treatment rescues neonatal brain injury. *Nature* **506**, 230-234 (2014). https://doi.org/10.1038/nature12880

49 Uludag, K. & Roebroeck, A. General overview on the merits of multimodal neuroimaging data fusion. *Neuroimage* **102 Pt 1**, 3-10 (2014). https://doi.org/10.1016/j.neuroimage.2014.05.018

50 Suk, H. I., Lee, S. W., Shen, D. & Alzheimer's Disease Neuroimaging, I. Latent feature representation with stacked auto-encoder for AD/MCI diagnosis. *Brain Struct Funct* **220**, 841-859 (2015). https://doi.org/10.1007/s00429-013-0687-3

51 Pozniak, C. D. *et al.* Sox10 directs neural stem cells toward the oligodendrocyte lineage by decreasing Suppressor of Fused expression. *Proc Natl Acad Sci U S A* **107**, 21795-21800 (2010). https://doi.org/10.1073/pnas.1016485107

52 Takada, N., Kucenas, S. & Appel, B. Sox10 is necessary for oligodendrocyte survival following axon wrapping. *Glia* **58**, 996-1006 (2010). https://doi.org/10.1002/glia.20981

53 Gabriel, L. A. *et al.* ADAMTSL4, a secreted glycoprotein widely distributed in the eye, binds fibrillin-1 microfibrils and accelerates microfibril biogenesis. *Invest Ophthalmol Vis Sci* **53**, 461-469 (2012). https://doi.org/10.1167/iovs.10-5955

54 Tawk, M. *et al.* Wnt/beta-catenin signaling is an essential and direct driver of myelin gene expression and myelinogenesis. *J Neurosci* **31**, 3729-3742 (2011). https://doi.org/10.1523/JNEUROSCI.4270-10.2011

55 Zheng, H. F. *et al.* WNT16 influences bone mineral density, cortical bone thickness, bone strength, and osteoporotic fracture risk. *PLoS Genet* **8**, e1002745 (2012). https://doi.org/10.1371/journal.pgen.1002745

56 de Araujo Tavares, M. E. *et al.* Refining patterns of MEF2C effects in white matter microstructure and psychiatric features. *J Neural Transm (Vienna)* **130**, 697-706 (2023). https://doi.org/10.1007/s00702-023-02626-5

57 Harrison, P. J. & Bannerman, D. M. GRIN2A (NR2A): a gene contributing to glutamatergic involvement in schizophrenia. *Mol Psychiatry* **28**, 3568-3572 (2023). https://doi.org/10.1038/s41380-023-02265-y

58 Harrington, A. J. *et al.* MEF2C Hypofunction in Neuronal and Neuroimmune Populations Produces MEF2C Haploinsufficiency Syndrome-like Behaviors in Mice. *Biol Psychiatry* **88**, 488-499 (2020). https://doi.org/10.1016/j.biopsych.2020.03.011

59 Feinstein, D. L. *et al.* Peroxisome proliferator-activated receptor-gamma agonists prevent experimental autoimmune encephalomyelitis. *Ann Neurol* **51**, 694-702 (2002). https://doi.org/10.1002/ana.10206

60 Cash, A. & Theus, M. H. Mechanisms of Blood-Brain Barrier Dysfunction in Traumatic Brain Injury. *Int J Mol Sci* **21** (2020). https://doi.org/10.3390/ijms21093344

61 Miller, K. L. *et al.* Multimodal population brain imaging in the UK Biobank prospective epidemiological study. *Nat Neurosci* **19**, 1523-1536 (2016). https://doi.org/10.1038/nn.4393

62 Wainberg, M. *et al.* Genetic architecture of the structural connectome. *Nat Commun* **15**, 1962 (2024). https://doi.org/10.1038/s41467-024-46023-2

63 Wang, C. *et al.* Phenotypic and genetic associations of quantitative magnetic susceptibility in UK Biobank brain imaging. *Nat Neurosci* **25**, 818-831 (2022). https://doi.org/10.1038/s41593-022-01074-w

64 Ritchie, J., Pantazatos, S. P. & French, L. Transcriptomic characterization of MRI contrast with focus on the T1-w/T2-w ratio in the cerebral cortex. *Neuroimage* **174**, 504-517 (2018). https://doi.org/10.1016/j.neuroimage.2018.03.027

65 Sudlow, C. *et al.* UK biobank: an open access resource for identifying the causes of a wide range of complex diseases of middle and old age. *PLoS Med* **12**, e1001779 (2015). https://doi.org/10.1371/journal.pmed.1001779

66 Andersson, J. L. R. & Sotiropoulos, S. N. An integrated approach to correction for off-resonance effects and subject movement in diffusion MR imaging. *Neuroimage* **125**, 1063-1078 (2016). https://doi.org/10.1016/j.neuroimage.2015.10.019

67 Gaser, C. *et al.* CAT: a computational anatomy toolbox for the analysis of structural MRI data. *Gigascience* **13** (2024). https://doi.org/10.1093/gigascience/giae049

68 Bycroft, C. *et al.* The UK Biobank resource with deep phenotyping and genomic data. *Nature* **562**, 203-209 (2018). https://doi.org/10.1038/s41586-018-0579-z

69 Purcell, S. *et al.* PLINK: a tool set for whole-genome association and population-based linkage analyses. *Am J Hum Genet* **81**, 559-575 (2007). https://doi.org/10.1086/519795

70 Guo, B. *et al.* Efficient multi-phenotype genome-wide analysis identifies genetic associations for unsupervised deep-learning-derived high-dimensional brain imaging phenotypes. *medRxiv* (2024). https://doi.org/10.1101/2024.12.06.24318618

71 Zhang, L. *et al.* ADHDgene: a genetic database for attention deficit hyperactivity disorder. *Nucleic Acids Res* **40**, D1003-1009 (2012). https://doi.org/10.1093/nar/gkr992

72 Basu, S. N., Kollu, R. & Banerjee-Basu, S. AutDB: a gene reference resource for autism research. *Nucleic Acids Res* **37**, D832-836 (2009). https://doi.org/10.1093/nar/gkn835

73 Satterstrom, F. K. *et al.* Large-Scale Exome Sequencing Study Implicates Both Developmental and Functional Changes in the Neurobiology of Autism. *Cell* **180**, 568-584 e523 (2020). https://doi.org/10.1016/j.cell.2019.12.036

74 Allen, N. C. *et al.* Systematic meta-analyses and field synopsis of genetic association studies in schizophrenia: the SzGene database. *Nat Genet* **40**, 827-834 (2008). https://doi.org/10.1038/ng.171

75 Pinero, J. *et al.* The DisGeNET knowledge platform for disease genomics: 2019 update. *Nucleic Acids Res* **48**, D845-D855 (2020). https://doi.org/10.1093/nar/gkz1021

76 Bertram, L., McQueen, M. B., Mullin, K., Blacker, D. & Tanzi, R. E. Systematic meta-analyses of Alzheimer disease genetic association studies: the AlzGene database. *Nat Genet* **39**, 17-23 (2007). https://doi.org/10.1038/ng1934

77 Nalls, M. A. *et al.* Large-scale meta-analysis of genome-wide association data identifies six new risk loci for Parkinson's disease. *Nat Genet* **46**, 989-993 (2014). https://doi.org/10.1038/ng.3043

78 Pinero, J. *et al.* DisGeNET: a comprehensive platform integrating information on human disease-associated genes and variants. *Nucleic Acids Res* **45**, D833-D839 (2017). https://doi.org/10.1093/nar/gkw943

79 Pearl, J. R. *et al.* Genome-Scale Transcriptional Regulatory Network Models of Psychiatric and Neurodegenerative Disorders. *Cell Syst* **8**, 122-135 e127 (2019). https://doi.org/10.1016/j.cels.2019.01.002

80 Zhu, Y. *et al.* Spatiotemporal transcriptomic divergence across human and macaque brain development. *Science* **362** (2018). https://doi.org/10.1126/science.aat8077

81 Cannon, M. *et al.* DGIdb 5.0: rebuilding the drug-gene interaction database for precision medicine and drug discovery platforms. *Nucleic Acids Res* **52**, D1227-D1235 (2024). https://doi.org/10.1093/nar/gkad1040

82 Shannon, P. *et al.* Cytoscape: a software environment for integrated models of biomolecular interaction networks. *Genome Res* **13**, 2498-2504 (2003). https://doi.org/10.1101/gr.1239303